



## Research articles

Exchange-biased SiO<sub>2</sub>/Co/CoO granular multilayers deposited by sequential sputteringM. Gamino<sup>a,b,\*</sup>, S. Michea<sup>c</sup>, J.C. Denardin<sup>c</sup>, L.F. Schelp<sup>b</sup>, M.A. Correa<sup>d</sup>, F. Bohn<sup>d</sup>, L.S. Dorneles<sup>b</sup><sup>a</sup> Departamento de Física, Universidade Federal de Pernambuco, 50670-901 Recife, PE, Brazil<sup>b</sup> Universidade Federal de Santa Maria, Departamento de Física, Av. Roraima, 1000, Bairro Camobi, 97105-900 Santa Maria, RS, Brazil<sup>c</sup> Universidad de Santiago de Chile, Avda. Ecuador, 3493, Estacion Central, Santiago, Chile<sup>d</sup> Departamento de Física, Universidade Federal do Rio Grande do Norte, 59078-900 Natal, RN, Brazil

## ARTICLE INFO

## Article history:

Received 8 March 2017

Accepted 19 April 2017

Available online 4 May 2017

## Keywords:

Magnetic properties

Exchange bias

Extraordinary Hall effect

Granular multilayers

## ABSTRACT

We investigate the magnetic properties in a system engineered to present Co grains laterally surrounded by a CoO matrix. By considering ferromagnetic SiO<sub>2</sub>/Co/CoO granular multilayers produced by sequential sputtering deposition, we verify that the Co grains present strong interfacial exchange coupling with the CoO matrix, assigned by the exchange bias effect as well as the raise of the Co blocking temperature. Moreover, through magnetization and Hall resistivity experiments, we observe that the antiferromagnetic ordering temperature and exchange bias are dependent on the thickness of the antiferromagnetic material, attributed to finite size effects, as well as we find that the Co blocking temperature is raised as the CoO layer becomes thicker. We discuss the experimental results in terms of the growth mode of the layers, morphological properties of the multilayers, and temperature dependence of the magnetic behavior. The results place the sequential sputtering deposition as a promising alternative technique to produce Co/CoO granular multilayers.

© 2017 Elsevier B.V. All rights reserved.

## 1. Introduction

The exchange bias (EB) effect is primarily characterized by the displacement of the magnetic hysteresis loop along the magnetic field axis [1,2]. The effect is observed in systems exhibiting the exchange interaction at the interface between a ferromagnetic material and an antiferromagnet [1,2], ferrimagnet [3], or a spin glass [4]. Although extensively employed in sensor elements of technological devices to shift the giant or tunnel magnetoresistance response [5], or in magnetic memories of reduced dimensions to stabilize the magnetization [6], the EB effect is still one of the most studied topics in condensed matter physics [7]. In particular, it is of great interest from the point of view of fundamental physics, due to the complexity of the magnetic coupling at the interface between the two materials [5]; for instance, in polycrystalline thin films there might exist regions with uncompensated spins which behave as single ferromagnetic domains and interact with the adjacent ferromagnetic and/or antiferromagnetic grains [8–11].

Despite the EB effect has been observed for the first time in partially oxidized Co fine particles [6], it has been investigated in several systems since its discovery [5,6]. From the seminal report of Skumryev et al. [12], in the last decade the interest on the EB effect in nanoparticles has reemerged and large efforts have been devoted to its investigation [13,14]. This interest is particularly motivated by the large exchange anisotropy field found for the nanoparticles exhibiting exchange bias, ~ 1 T [15], the thermal stability of the nanoparticles [16,17], the possibility to enhance the superparamagnetic blocking temperature [18], and by the wide variety of structures that can be experimentally tested, such as Co core grains with CoO shells [13,19,12], Co grains inside a CoO matrix [12], as well as several types of bi-, tri- or multi-layers [10,20–23].

Important results for nanoparticles exhibiting EB have been found in two different systems: (i) Co grains with CoO shells inside a CoO matrix [19,12]; (ii) pure granular CoO, where non-zero net magnetization comes from defectively compensated spins near the grain boundaries [24], structural defects [25], or local variations of stoichiometry [26]. In the first case, the exchange anisotropy is tuned by direct coupling between uncompensated spins of the antiferromagnet's surface. In the second case, the net moment is effective even above the Néel temperature, and the magnetic coupling is governed by local disorder and frustration,

\* Corresponding author at: Departamento de Física, Universidade Federal de Pernambuco, 50670-901 Recife, PE, Brazil.

E-mail address: [mgaminogomes@gmail.com](mailto:mgaminogomes@gmail.com) (M. Gamino).

a spin-glass-like behavior [27]. Irrespective of the structural arrangement of the two materials, an important part of the effect is due to the magnetic properties of the CoO. In Co/CoO core-shell structures, the strains at the interface along specific crystallographic directions affect not only the core/shell magnetic coupling, but also bring the CoO Néel temperature down to  $\sim 235$  K, well below the value verified for bulk systems,  $\sim 293$  K [28]. In this case, finite size effects associated to the CoO shell dimension seem to be less pronounced than those found in multilayers where CoO films are intercalated with non-magnetic films [29,24]. When in contact with a ferromagnet, CoO finite size effects seem to play an important role also in Co/CoO bilayers [30]. Possibly due to the absence of significant strain in multilayers, the Néel temperature can be tuned from  $\sim 220$  K up to values near those found for bulk materials, depending on the average grain size and the CoO layer thickness.

In this work, we investigate the magnetic properties and exchange bias effect in a system engineered to present Co grains laterally surrounded by the CoO matrix. We consider ferromagnetic  $\text{SiO}_2/\text{Co}/\text{CoO}$  granular multilayers produced by sequential sputtering deposition, and verify the morphological properties, through transmission electron microscopy, as well as the magnetic behavior, via temperature dependence of the magnetization, Hall resistivity, and magnetization curves. We show that the Co grains present strong interfacial exchange coupling with the CoO matrix. Moreover, we observe a dependence of the blocking temperature and exchange bias field with the thickness of the antiferromagnetic layer, as well as the raise of the Co blocking temperature as the CoO layer becomes thicker. The results place the sequential sputtering deposition as a promising alternative technique to produce Co/CoO granular multilayers.

## 2. Experiment

For the study, we prepare sets of ferromagnetic multilayers by sequential sputtering deposition. The first two sets are  $[\text{SiO}_2(2.0\text{ nm})/\text{Co}(1.0\text{ nm})] \times 10$  and  $[\text{CoO}(t_{\text{CoO}})/\text{Co}(1.0\text{ nm})] \times 10$  multilayers, where  $t_{\text{CoO}}$  is the thickness of the CoO layers. The knowledge of the morphology of the first two sets is important to justify the deposition route employed to the production of the other multilayers. These consist of  $[\text{SiO}_2(2.0\text{ nm})/\text{Co}(1.0\text{ nm})/\text{CoO}(t_{\text{CoO}})] \times 10$  and  $[\text{SiO}_2(2.0\text{ nm})/\text{Co}(t_{\text{Co}})/\text{CoO}(4.0\text{ nm})] \times 10$  multilayers, where  $t_{\text{Co}}$  is the thickness of the Co layers. For all sets, the nominal thickness  $t_{\text{Co}}$  of the Co layers is below 1.75 nm, which is the thickness found to produce a continuous Co film onto  $\text{SiO}_2$  [31], the thickness  $t_{\text{CoO}}$  of the CoO layer varies from 1.0 to 4.0 nm, and the thickness of the  $\text{SiO}_2$  layers is 2.0 nm. A 10 nm-thick  $\text{SiO}_2$  buffer layer is deposited onto the substrate before the sequential deposition, while a 4 nm-thick  $\text{SiO}_2$  cap layer covers the multilayers.

The samples are deposited by magnetron sputtering onto  $\langle 111 \rangle \text{Si}$  substrates with thermally oxidized surfaces, using  $\text{SiO}_2$ , Co, and CoO targets, under the following conditions: base pressure of  $1 \times 10^{-7}$  Torr, deposition pressure of  $2.0 \times 10^{-3}$  Torr with 99.99% pure Ar at 32 sccm constant flow, DC power source for the deposition of the Co layers, and RF power source for the CoO and  $\text{SiO}_2$  layers. Under these conditions, the deposition rates for  $\text{SiO}_2$ , Co, and CoO layers are 0.06 nm/s, 0.11 nm/s, and 0.09 nm/s, respectively.

The morphological properties of the multilayers are obtained via cross-section transmission electron microscopy (TEM), in the bright field imaging mode, using a JEOL JEM-3010 ARP microscope.

The magnetic characterization is performed via magnetization curves, temperature dependence of field-cooled (FC) and zero-field-cooled (ZFC) magnetization, and Hall resistivity. The first two experiments are carried out using a Quantum Design SQUID

magnetometer. In particular, the magnetization curves are measured at specific temperatures after field cooling down to 10 K with 30 kOe applied in the plane of the multilayer, while the FC and ZFC magnetization measurements are acquired in the range of temperature between 10 K and 300 K, under a constant field of 200 Oe.

The Hall resistivity experiments are performed using a home-made system, in which the sample is inside a Displex DMX-19 closed cycle cryostat, and the electric measurement is carried out in the Van der Pauw geometry using a Keithley nanovoltmeter, an AC/DC current source, and a  $6 \times 8$  matrix card. In this case, Hall resistivity curves are acquired at specific temperatures in the range between 10 to 300 K, after zero field cooling and field cooling down to 10 K, the latter with 5 kOe applied normal to the plane of the multilayer.

## 3. Results and discussion

Fig. 1 presents transmission electron microscopy images from selected ferromagnetic multilayers. It can be clearly verified that the growth mode of the Co layers is quite different when deposited onto  $\text{SiO}_2$  or CoO. For the  $\text{SiO}_2$  matrix, due to the difference of surface free energy between Co and silicon oxide ( $1857 \text{ erg/cm}^2$  and  $307\text{--}605 \text{ erg/cm}^2$ , respectively [32]), the Stranski–Krastanov growth mode of Co onto  $\text{SiO}_2$  is favored, forming essentially spherical Co grains with mean diameter of around 3 nm, identified through the dark field in the image of Fig. 1(a). On the other hand for the CoO matrix, as shown in Fig. 1(b), the Co grains appear just in the first and part of the second layers. This fact is probably a consequence of non-continuous CoO layer formed when CoO is deposited onto  $\text{SiO}_2$ , which allows the arrival of the Co atoms over the silicon oxide surface. For the subsequent Co depositions, the atoms wet the surface and cover the CoO, forming a continuous film or platelet-like aggregates. This evolution from the Stranski–Krastanov growth mode to the Volmer–Weber one, when  $\text{SiO}_2$  is replaced by CoO, reflects the energy balance of the surface energies. This balance is much more favorable for Co grains formation in  $\text{SiO}_2$  than in CoO [32]. For both sets of samples, at least part of the CoO forms f.c.c. crystals that extend themselves over several bi-layers, imposing the f.c.c. structure to the Co layers. Therefore, under our experimental conditions, either the Co does not form spherical clusters when deposited onto CoO, or it happens only for a nominal thickness smaller than that usually found for Co layers grown onto  $\text{SiO}_2$ . As below this critical value the size of the cluster scales with the nominal thickness, even if spherical Co cluster would be created, they should be limited to small diameters.

These results show a route to obtain samples consisting of Co grains laterally surrounded by a CoO matrix. Thus, in order to combine the main features of both sets of samples, we use sequential sputtering deposition to produce the  $\text{SiO}_2/\text{Co}/\text{CoO}$  granular multilayers. Fig. 1(c) presents a TEM image for the  $\text{SiO}_2/\text{Co}/\text{CoO}$  multilayer with  $t_{\text{CoO}} = 3.0$  nm, as a representative example of the general structure verified for this set. By interposing a  $\text{SiO}_2$  layer before each Co deposition, the cluster formation is guaranteed. In the subsequent CoO deposition, the deposited material fills the empty space between Co grains and, if the CoO film is thick enough, covers these grains. This is verified through the inset of the image, in which a granular multilayer is formed by Co grains (dark field), CoO layers (gray field), and  $\text{SiO}_2$  spacer (white field). In all cases, the Co grains are asymmetrically surrounded by the CoO, as the metallic Co is deposited onto  $\text{SiO}_2$ . Since the nominal thickness of each layer is chosen independently, the distance between successive Co/CoO layers, the morphology of the Co and the CoO layers, as well as the size of the Co grains may be controlled.

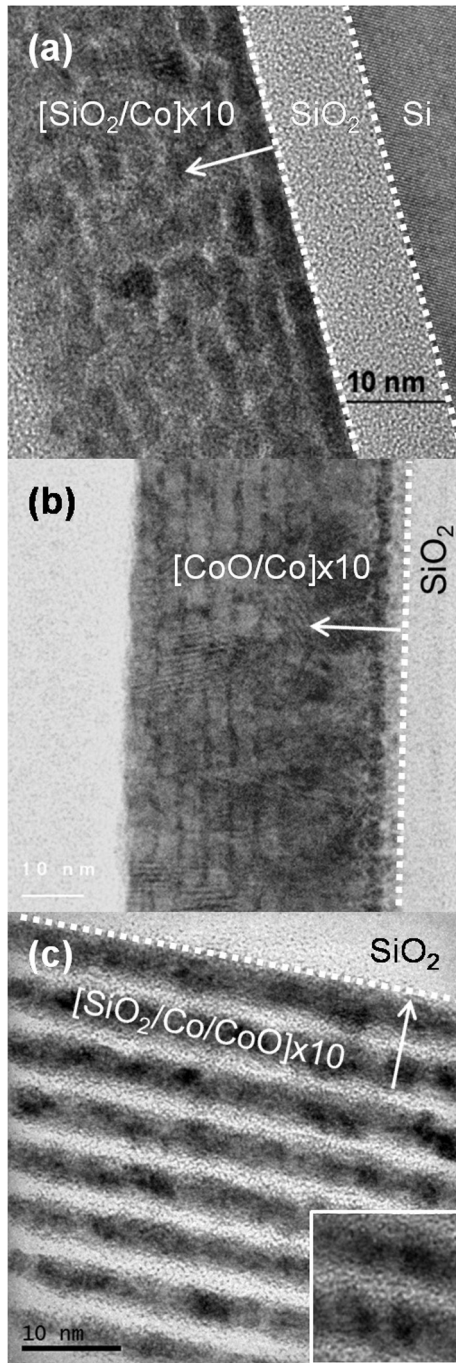


**Fig. 1.** Cross-section TEM images for the (a)  $\text{SiO}_2(2.0 \text{ nm})/\text{Co}(1.0 \text{ nm})$ , (b)  $\text{CoO}(3.5 \text{ nm})/\text{Co}(1.0 \text{ nm})$ , and (c)  $\text{SiO}_2(2.0 \text{ nm})/\text{Co}(1.0 \text{ nm})/\text{CoO}(3.0 \text{ nm})$  multilayers. The inset in (c) shows a detailed view of the Co (dark field) and CoO (gray field) counterparts. The white arrows indicate the growth direction of the multilayers.

Figs. 2 and 3 present the magnetization behavior as a function of the temperature for the ZFC and FC cycles of selected multilayers. For the  $\text{SiO}_2/\text{Co}$  multilayer, Fig. 2(a), the curves indicate the Co blocking temperature of  $T_B \sim 140 \text{ K}$ , the temperature at which superparamagnetism sets in. Below  $T_B$ , the FC and ZFC magnetization curves are split, whereas above  $T_B$ , they coincide as the remanence and coercivity vanish. Actually, this behavior is expected given the morphology of the sample, i.e. Co grains with mean diameter of  $\sim 3 \text{ nm}$ . On the other hand, for the  $\text{CoO}/\text{Co}$  multilayer with  $t_{\text{CoO}} = 3.5 \text{ nm}$ , Fig. 2(b), the FC and ZFC magnetization curves exhibit a completely different behavior, with a peak at the Néel

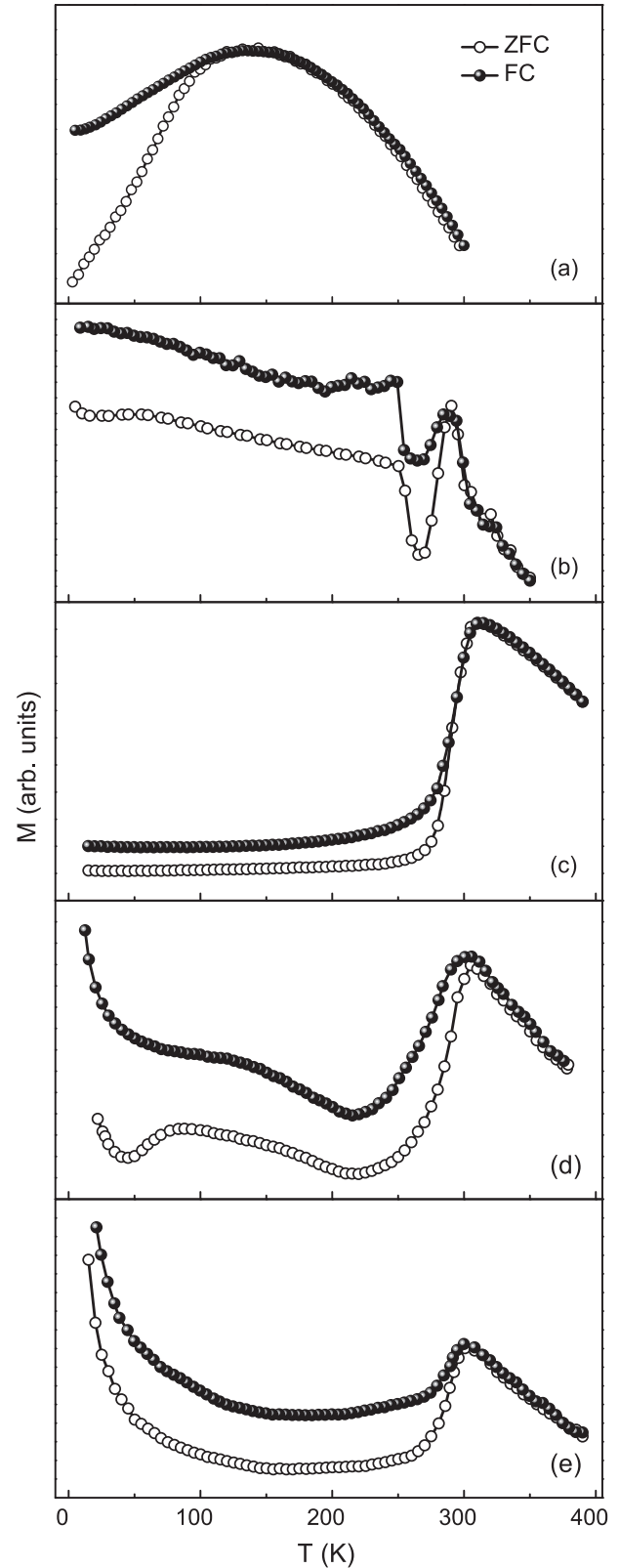


**Fig. 2.** Temperature dependence of the ZFC and FC magnetization for the (a)  $\text{SiO}_2/\text{Co}(1.0 \text{ nm})$ , (b)  $\text{CoO}(3.5 \text{ nm})/\text{Co}(1.0 \text{ nm})$ , and for the  $\text{SiO}_2/\text{Co}(t_{\text{Co}})/\text{CoO}(4.0 \text{ nm})$  multilayers with (c)  $t_{\text{Co}} = 1.5 \text{ nm}$ , (d)  $1.0 \text{ nm}$ , and (e)  $0.7 \text{ nm}$ .

temperature of the CoO,  $T_N = 293 \text{ K}$ , indicating that the magnetization is sensitive to the antiferromagnetic order of the insulator. However, they do not present any classical evidence for a super-



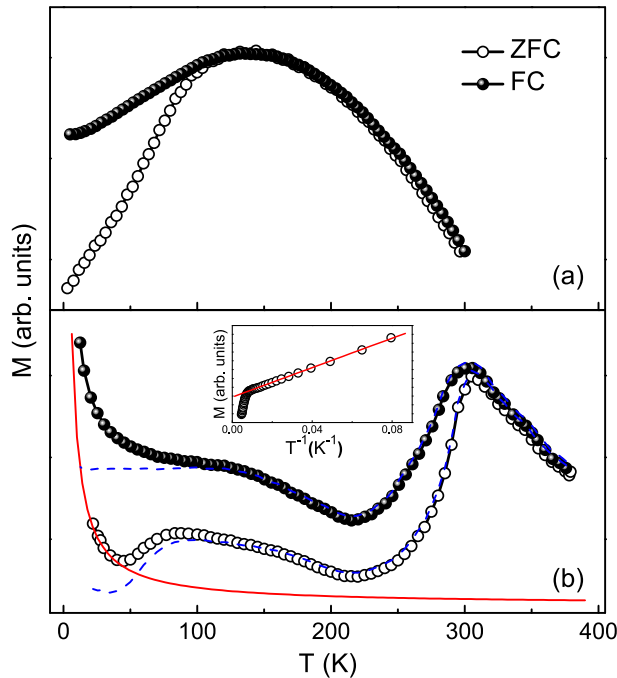


**Fig. 3.** Temperature dependence of the ZFC and FC magnetization for the (a)  $\text{SiO}_2/\text{Co}(1.0 \text{ nm})$  and (b)  $\text{SiO}_2/\text{Co}(1.0 \text{ nm})/\text{CoO}(4.0 \text{ nm})$  multilayers. In (b) it is possible to observe the behavior predicted by the Curie Law of the magnetic contribution from the *molecular* Co. The solid red line corresponds to the behavior predicted by the Curie Law, while the dashed blue ones are the experimental ZFC and FC magnetization curves after the extraction of the magnetic contribution of the *molecular* Co obtained through the Curie Law. Moreover, the inset presents the experimental FC magnetization as a function of the inverse of temperature, for a low temperature range, together with fit of the data, represented by the solid red line, obtained using the Curie Law.

paramagnetic transition. Since the sample consists of a mixture of morphologies, with a smaller fraction of Co platelet-like aggregates when compared to the one for continuous film, this behavior becomes reasonable.

The most striking findings here reside in the magnetic characterization of the  $\text{SiO}_2/\text{Co}/\text{CoO}$  granular multilayers produced by sequential sputtering deposition. For the multilayers with  $t_{\text{Co}}$  below 1.5 nm, Fig. 2(d) and (e), the FC and ZFC magnetization curves show a rather complex structure. In this case, diverse magnetic contributions affecting the whole magnetic behavior can be identified. It is possible to observe in the curves the huge increase of the magnetization when the temperature approaches its lower limit. In particular, this contribution is due to small clusters containing just a few Co atoms, sometimes also referred as *molecular* Co [33], that remain in the superparamagnetic state even at very low temperatures. The Co clusters, that besides influencing the average size of the Co grains, interfere significantly in the magnitude of the effective anisotropy of nanoparticles, since they contribute to an increase of the surface anisotropy [34]. The increase may also be associated to defects in the antiferromagnetic material, that lead to uncompensated moments due to the oxygen deficiency. The Co clusters arise from the Co atoms that during the deposition do not present energy enough to move and to achieve the centers of coalescence or nucleation that give rise to the larger clusters, as well as they also appear from local deviation from stoichiometry in the CoO. The presence of small Co clusters has been previously verified in granular films deposited by sputtering [34], and they are evidenced through a discrepancy between the amount of Co deposited over the  $\text{Al}_2\text{O}_3$  layer and the amount that is quantified by TEM images [35].

Anyway, given that our focus resides in the granular contribution of the sample, it is useful to discount the paramagnetic response at  $T \rightarrow 0$ . The magnetic contribution of the small Co clusters can be assessed by plotting the FC magnetization as a function of the inverse of temperature, for a low temperature range, as shown in the inset of Fig. 3(b). Here, we employ the Curie law to fit the experimental data in the low temperature range, from 0.01 to 0.08  $\text{K}^{-1}$ , corresponding to the *molecular* Co, and then extract this contribution from the FC and ZFC magnetization curves, following the procedure reported in Ref. [33]. The resulting curves, after the removal, as well as the Curie Law prediction, are also shown in Fig. 3(b). In particular, the subtraction has negligible influence on the curves above  $\sim 100 \text{ K}$ . However, the expected behavior for superparamagnetic particles, i.e. a decrease towards zero of the ZFC magnetization below the blocking temperature, is recovered. Notice that it is found at around 140 K, quite close to the ferromagnetic Co blocking temperature  $T_B$  verified for the  $\text{SiO}_2/\text{Co}$  multilayer (Figs. 2(a) and 3(a)).

With respect to the CoO response, the magnetic behavior is mainly revealed in a wide range of the FC and ZFC magnetization curves at high temperatures. When the CoO nominal thickness is higher than the Co nominal thickness, which are the cases presented in Fig. 2(c–e), the magnetization increases for both curves as the temperature decreases from the upper temperature limit, reaching a maximum at around 300 K. Below this temperature, the FC and ZFC curves split as the antiferromagnetic order starts to be progressively established in the CoO grains.

In particular, for the samples in which just CoO is present, such as the one shown in Fig. 2(b), the central position of the peak and its width are related to the blocking temperature and to the grain size distribution of the antiferromagnet, respectively [29,24,25]. Thus, the same reasoning can be applied here, at least when the amount of CoO is larger than the amount of Co. Moreover, it is important to point out that the blocking temperature  $T_B$  of the CoO decreases as the thickness decreases [25,29,36,29,24,25,28], since the size of the CoO grain is limited by the nominal thickness.

It is well-known that magnetic properties, i.e. the magnetic behavior of the different materials constituting the multilayers, play a fundamental role in the Hall resistivity response. Since the magnitude of the extraordinary Hall effect is proportional to the magnetization, it reflects the main features of the magnetic hysteresis loop [37,38]. In this sense, Hall resistivity experiments cor-

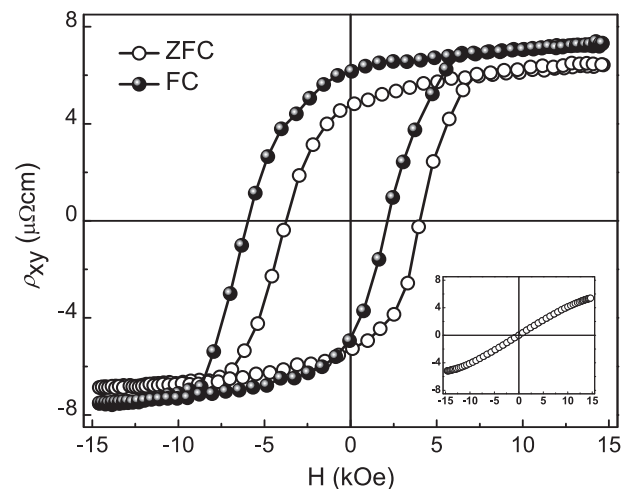


**Fig. 4.** Hall resistivity measurements, obtained after the ZFC and FC processes, at 70 K for the  $\text{SiO}_2/\text{Co}(1.0 \text{ nm})/\text{CoO}(3.0 \text{ nm})$  multilayer. The inset present the Hall resistivity curve at room temperature.

respond to a complementary and promising technique to investigate the properties of magnetic materials.

Regarding the Hall resistivity results, Fig. 4 shows the Hall resistivity measurements obtained after the ZFC and FC processes, as a function of the magnetic field applied *normal* to the film plane, for the  $\text{SiO}_2/\text{Co}(1.0 \text{ nm})/\text{CoO}(3.0 \text{ nm})$  multilayer, as a representative example of the curves acquired for the set. At room temperature, the samples present curves characterized by remanent signal and coercive field equal to zero, as shown in the inset of Fig. 4, a typical behavior of superparamagnets. However, below the respective superparamagnetic blocking temperature, the samples exhibit ferromagnetic-like loops, as expected, reflecting the blocked state.

Our results raise an interesting issue on the Hall resistivity behavior and the magnetic interactions acting in our multilayers. Generally, our films consist of ferromagnetic Co grains laterally surrounded by an antiferromagnetic CoO matrix. Thus, we interpret our experimental data as a clear evidence of the exchange interaction acting at the interface between the ferromagnetic material and the antiferromagnet. The exchange coupling is primarily assigned here by the shift in field of the loop in the Hall resistivity measurement after field cooling, as well as by the increase of the remanent signal and the coercive field, when compared to the results verified for the Hall resistivity after zero field cooling.

In this system, the exchange bias effect emerges from two sources: (i) lateral exchange bias [39] due to the CoO surrounding the Co grains and (ii) antiferromagnetic thickness dependence of exchange bias from the CoO layer in the top of the grains [40]. The exchange bias effect is strongly dependent on the nominal thickness of the CoO, as well as on its magnetic state. Fig. 5 presents the temperature dependence of the effective exchange bias field  $H_{\text{eb}}$ , and coercive field  $H_c$ , obtained from the Hall resistivity measurements after FC process, for  $\text{SiO}_2/\text{Co}(1.0 \text{ nm})/\text{CoO}$  multilayers with distinct  $t_{\text{CoO}}$  values. The exchange coupling between the ferromagnetic Co grains and the antiferromagnetic CoO matrix becomes more evident as the thickness of the CoO layer increases. In particular, notice that the amplitude of both  $H_{\text{eb}}$  and  $H_c$ , at a given temperature value at the low temperatures range, increases as the CoO is thicker, as expected. Moreover, the temperature dependence of  $H_{\text{eb}}$  and  $H_c$  experimental data may indicate  $T_{H_{\text{eb}}}$  and  $T_{H_c}$ , the temperatures where the exchange bias and coercive fields become zero, respectively. In this case, it is possible to verify that both values also increase as the CoO is thicker. This behavior is a consequence of finite size effects that become more evident for smaller CoO grain size.

Usually, the CoO  $T_B$  is highly influenced by stoichiometry of the antiferromagnet, and its increase confirms that the thicker CoO is rather well-defined, with considerable magnetic anisotropy. The temperature dependence of the  $H_{\text{eb}}$  and  $H_c$  behavior can be understood in terms of the contact interface area between the Co grains, which is related with the stability of the CoO matrix surrounding the Co grains. For a conventional ferro/antiferromagnetic system, the evolution of  $H_{\text{eb}}$  with the thickness of the ferromagnet  $t_{\text{fm}}$  is given by a function of the type  $H_{\text{eb}} \propto 1/t_{\text{fm}}$ , i.e. it is directly dependent on the Co thickness. Thus, we may assume that any change in the  $H_{\text{eb}}$  is related to the CoO antiferromagnetic order, since the Co thickness is kept constant in our multilayers. In particular, for the  $\text{SiO}_2/\text{Co}(1.0 \text{ nm})/\text{CoO}$  multilayer with  $t_{\text{CoO}} = 3.0 \text{ nm}$ , Fig. 5(a),  $T_{H_{\text{eb}}} \sim T_{H_c} \sim 200 \text{ K}$ , while for  $t_{\text{CoO}} = 2.0 \text{ nm}$ , Fig. 5(b),  $T_{H_{\text{eb}}} \sim T_{H_c} \sim 150 \text{ K}$ . Notice that  $T_{H_{\text{eb}}}$  and  $T_{H_c}$  are above  $100 \text{ K}$ , the Co  $T_B$  verified in Fig. 3(b), a fact directly related to the Co grain size dispersion in the  $\text{SiO}_2/\text{CoO}$  matrix. For the multilayer with  $t_{\text{CoO}} = 1.0 \text{ nm}$ , Fig. 5(c), although  $H_c$  raises from a temperature  $T_{H_c}$  below  $100 \text{ K}$ , none shift of the loop is observed even for measurements at temperatures as low as  $12 \text{ K}$ . This raise of the  $H_c$  may

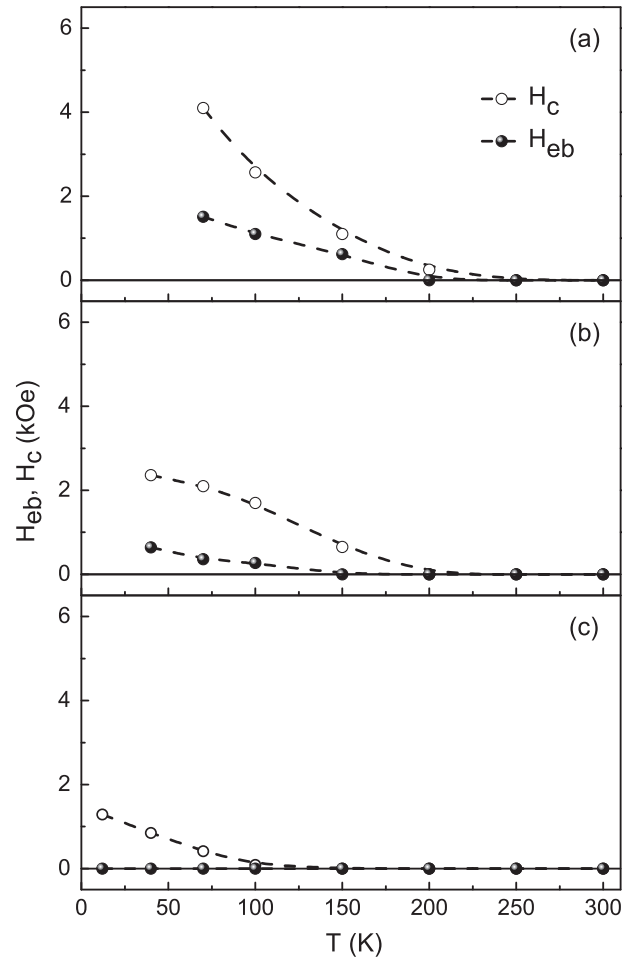


Fig. 5. Temperature dependence of the effective exchange bias field  $H_{\text{eb}}$  and coercive field  $H_c$ , obtained from the Hall resistivity measurements after FC process, for the  $\text{SiO}_2/\text{Co}(1.0 \text{ nm})/\text{CoO}(t_{\text{CoO}})$  multilayers with (a)  $t_{\text{CoO}} = 3.0 \text{ nm}$ , (b)  $2.0 \text{ nm}$ , and (c)  $1.0 \text{ nm}$ .

be observed even that the spins in the antiferromagnet revert the orientations together with the magnetic moments of the ferromagnet when the external magnetic field is applied, while that the  $H_{\text{eb}}$  needs an additional condition to happen, i.e. the antiferromagnetic order shall be stable against thermal fluctuations and also to the magnetic field applied during the experiments. Therefore, the  $H_{\text{eb}}$  appears just when a significant amount of CoO spins are antiferromagnetically ordered during the FC process. This way, a shift of the magnetization loop is noticed if the antiferromagnetic anisotropy is large, while if it is small, the observed effect is only an enhancement of the coercivity. In general, both effects can be observed simultaneously, mainly due to structural defects or grains size distribution, which alter the anisotropy [6].

These results obtained with the Hall resistivity experiments can be qualitatively compared to the ones acquired through conventional magnetization curves at specific temperatures, providing further insights on the magnetic properties of the multilayers, as well as confirming the strong exchange coupling between ferromagnetic Co grains and the antiferromagnetic CoO matrix.

Here, it is worth to point out that the Hall resistivity and magnetization measurements are performed under different fields configuration and experimental conditions. In particular, in contrast with what is usually done to acquire the magnetization curves, for the Hall resistivity measurement, the magnetic field applied during the cooling process is perpendicular to the sample plane,

and parallel to the field employed in the experiment. Thus, each technique may probe specific contribution of the ferro and antiferromagnetic anisotropy, and therefore some differences in the  $H_{eb}$  and  $H_c$  values, as well as in the  $T_{H_{eb0}}$  and  $T_{H_c}$  ones, become reasonable [41].

Fig. 6 shows the magnetization curves acquired at selected temperatures for the  $\text{SiO}_2/\text{Co}(1.0 \text{ nm})/\text{CoO}(3.0 \text{ nm})$  multilayer, as a representative example of the curves acquired for the set. In particular, the magnetization curves corroborate the general magnetic behavior of the multilayers verified through the Hall resistivity measurements. At room temperature, the shape of the magnetization curve and the zero value for the remanent magnetization and coercive field are fingerprints of the superparamagnetic state of the multilayer. In an ideal case, an assembly of isolated spherical grains, the results would be the same independently of the cooling magnetic field direction. But here, due to the dipolar coupling among Co grains, and possibly also due to contributions from crystalline anisotropy coming from preferential orientation during the sample growth, the easy magnetization axis is in the plane of the multilayer. This feature is clearly evidenced in the magnetization curves through the magnetic saturation, a fact not verified in the Hall resistivity results.

On the other hand, as the temperature is reduced, since the magnetization curves are acquired after a field cooling, the interaction between ferromagnetic Co grains and antiferromagnetic CoO is evidenced by the appearance of the exchange bias effect, verified through the shift of the hysteresis loop to negative fields. This strong exchange coupling can be attributed the stabilization of uncompensated spins on the surface of the nanoparticles, that is enhanced below the CoO Néel temperature. Moreover, the high-field behavior may be dominated higher orientation degree of the frozen surface spins of CoO with a possible polycrystalline nature, such as reported in Ref. [42].

We point out that the magnetization curves can be understood as a superposition of two effects, a standard hysteresis and a linear one. In particular, they are respectively devoted to two different ferromagnetic-like contributions, e.g., the ferromagnetic Co grains and the uncompensated spins in the CoO or the *molecular* Co. Remarkably, the latter becomes very large at low temperatures, leading to progressively smaller  $H_{eb}$  and  $H_c$  values. Thus, in order to obtain the intrinsic parameters related to the ferromagnetic phase, here, we remove this contribution by subtracting the linear

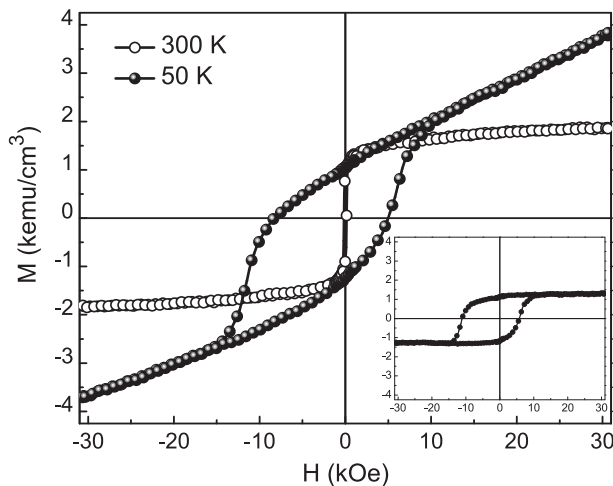


**Fig. 6.** Magnetization curves measured at 300 K and 50 K for the  $\text{SiO}_2/\text{Co}(1.0 \text{ nm})/\text{CoO}(3.0 \text{ nm})$  multilayer. In the inset, the resulting magnetization curve acquired at 50 K obtained after the subtraction of the linear contribution at high magnetic fields.

behavior of the magnetization curve at high magnetic field. The resulting curve, for instance at 50 K, is shown in the inset of Fig. 6.

From the resulting magnetization curves, Fig. 7 presents the temperature dependence of the  $H_{eb}$  and  $H_c$ , obtained from the magnetization curves acquired after a field cooling, for the  $\text{SiO}_2/\text{Co}(1.0 \text{ nm})/\text{CoO}$  multilayer with distinct  $t_{\text{CoO}}$  values. As the temperature is raised, both  $H_{eb}$  and  $H_c$  show a remarkable classical monotonic decrease. Moreover, it can be clearly noticed the raise of the blocking temperature of the Co grains, from 220 K up to 270 K, as the CoO thickness is varied from 1.0 nm to 3.0 nm CoO thickness. Both results corroborate the general magnetic behavior previously verified through the Hall resistivity experiments.

#### 4. Conclusion

In conclusion, we have investigated the magnetic properties and exchange bias effect in ferromagnetic  $\text{SiO}_2/\text{Co}/\text{CoO}$  granular multilayers produced by sequential sputtering deposition.

To this end, we have considered independently Hall resistivity and magnetization measurements, techniques which are performed under different fields configuration and experimental conditions. In this sense, the results suggest the Hall resistivity as a promising tool to investigate materials that, when combined with

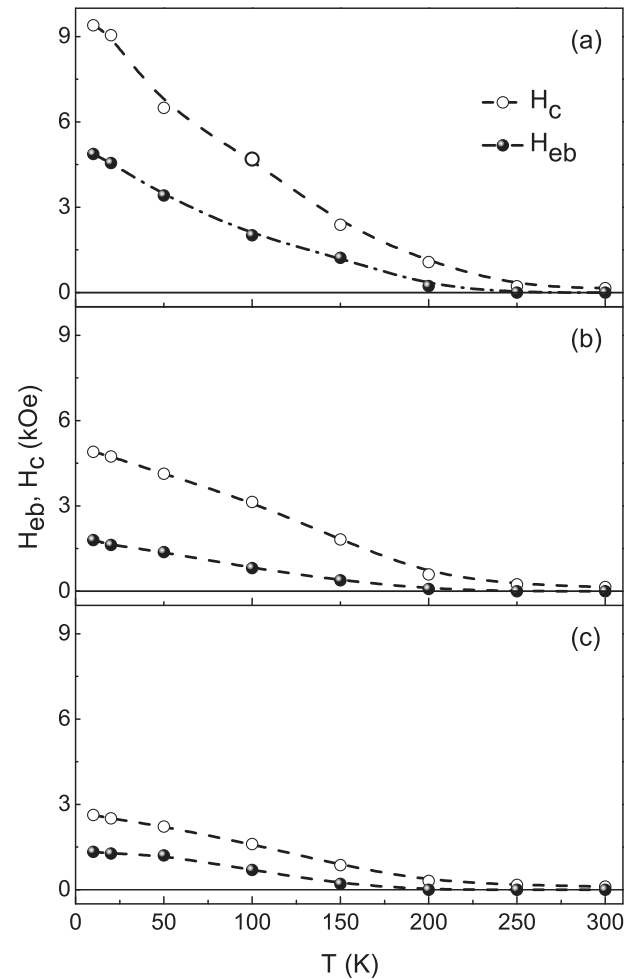


**Fig. 7.** Temperature dependence of the effective exchange bias field  $H_{eb}$  and coercive field  $H_c$ , obtained from the magnetization curves acquired after a field cooling, for the  $\text{SiO}_2/\text{Co}(1.0 \text{ nm})/\text{CoO}(t_{\text{CoO}})$  multilayers with (a)  $t_{\text{CoO}} = 3.0 \text{ nm}$ , (b)  $2.0 \text{ nm}$ , and (c)  $1.0 \text{ nm}$ . The  $H_{eb}$  and  $H_c$  are obtained from resulting magnetization curve obtained after the subtraction of the linear contribution at high magnetic fields.

conventional magnetization technique, may provide complementary insights on the magnetic properties.

From the results of both techniques, we have verified that in the engineered  $\text{SiO}_2/\text{Co}/\text{CoO}$  granular multilayers, the Co grains present strong interfacial exchange coupling with the CoO matrix. We have observed that the blocking temperature and exchange bias are dependent on the thickness of the antiferromagnetic material. Moreover, the Co blocking temperature raises as the CoO layer becomes thicker.

After all, it is worth to emphasize that the sequential sputtering deposition has allowed us to produce nanosized Co grains laterally surrounded by a CoO matrix and explore the exchange bias effect in a nanostructured engineered system. In general, cosputtering or coevaporation are the methods usually employed to obtain these granular solids, in which a random distribution of clusters in the matrix, with a large dispersion of grain sizes and distances, are verified [43]. On the other hand, the present alternative technique has provided us the complete control of the nanosized Co grains by varying the Co nominal thickness, independently on the  $\text{SiO}_2$  and CoO depositions, i.e. the distance between successive Co/CoO layers, the morphology of the Co and the CoO layers, the size of the Co grains, and, consequently, the magnetic properties of the system. In particular, it makes possible the production of Co nanoparticles close to percolation point, which favors the stronger exchange coupling between the ferromagnetic Co and the antiferromagnetic CoO, since the EB effect is enhanced by the quality of the interface. The results place the sequential sputtering deposition as a promising alternative technique to produce Co/CoO granular multilayers.

## Acknowledgments

This research is supported by the Brazilian agencies CNPq, CAPES, FACEPE and FAPERGS, and by the Chilean agencies Financiamiento Basal para Centros Científicos y Tecnológicos de Excelencia (CEDENNA), and Fondecyt 1140195.

## References

- [1] W.H. Meiklejohn, C.P. Bean, *Phys. Rev.* 102 (1956) 1413–1414.
- [2] W.H. Meiklejohn, C.P. Bean, *Phys. Rev.* 105 (1957) 904–913.
- [3] P. Prene, E. Tronc, J.-P. Jolivet, J. Livage, R. Cherkaoui, M. Nogues, J.-L. Dormann, D. Fiorani, *IEEE Trans. Magn.* 29 (1993) 2658–2660.
- [4] M. Ali, P. Adie, C.H. Marrows, D. Greig, B.J. Hickey, R.L. Stamps, *Nat. Mater.* 6 (2007) 70–75.
- [5] J. Nogués, I.K. Schuller, *J. Magn. Magn. Mater.* 192 (1999) 203–232.
- [6] J. Nogués, J. Sort, V. Langlais, V. Skumryev, S. Suriñach, J. Muñoz, M. Baró, *Phys. Rep.* 422 (2005) 65–117.
- [7] W.H. Meiklejohn, *J. Appl. Phys.* 33 (1962) 1328.
- [8] K. O'Grady, L. Fernandez-Outon, G. Vallejo-Fernandez, *J. Magn. Magn. Mater.* 322 (2010) 883–899.
- [9] A. Harres, J. Geshev, *J. Phys. Condens. Matter* 24 (2012) 326004.
- [10] A.E. Berkowitz, J.-I. Hong, S.K. McCall, E. Shipton, K.T. Chan, T. Leo, D.J. Smith, *Phys. Rev. B* 81 (2010) 134404.
- [11] M. Gamino, A.M.H. de Andrade, J.E. Schmidt, J. Geshev, *J. Phys. D Appl. Phys.* 47 (2014) 475001.
- [12] V. Skumryev, S. Stoyanov, Y. Zhang, G. Hadjipanayis, D. Givord, J. Nogués, *Nature* 423 (2003) 850–853.
- [13] J. Nogués, V. Skumryev, J. Sort, S. Stoyanov, D. Givord, *Phys. Rev. Lett.* 97 (2006) 157203.
- [14] M. Feyngenson, Y. Yiu, A. Kou, K.-S. Kim, M.C. Aronson, *Phys. Rev. B* 81 (2010) 195445.
- [15] D.L. Peng, K. Sumiyama, T. Hihara, S. Yamamuro, T.J. Konno, *Phys. Rev. B* 61 (2000) 3103–3109.
- [16] D. Givord, V. Skumryev, J. Nogués, *J. Magn. Magn. Mater.* 294 (2005) 111–116.
- [17] J.A. De Toro, D.P. Marques, P. Muñoz, V. Skumryev, J. Sort, D. Givord, J. Nogués, *Phys. Rev. Lett.* 115 (2015) 057201.
- [18] M. Gamino, J. de Oliveira, C. dos Santos, F. Bohn, L. Schelp, J. Denardin, *J. Magn. Magn. Mater.* 320 (2008) e308–e311.
- [19] D.L. Peng, K. Sumiyama, S. Yamamuro, T. Hihara, T.J. Konno, *Appl. Phys. Lett.* 74 (1999) 76.
- [20] T. Ambrose, C.L. Chien, *J. Appl. Phys.* 83 (1998) 6822.
- [21] M. Gruyters, D. Schmitz, *Phys. Rev. Lett.* 100 (2008) 077205.
- [22] R.B. da Silva, D.C. Viegas, V.P. Nascimento, M.A. Correa, L.F. Schelp, E. Baggio-Saitovitch, R.L. Sommer, *Appl. Phys. Lett.* 94 (2009) 042501.
- [23] R.B. da Silva, M.A. Corrêa, E.F. Silva, T.J.A. Mori, R.D. Della Pace, R. Dutra, A.D.C. Viegas, F. Bohn, R.L. Sommer, *Appl. Phys. Lett.* 104 (2014) 102405.
- [24] T. Ambrose, C. Chien, *Phys. Rev. Lett.* 76 (1996) 1743–1746.
- [25] M. Gruyters, *Phys. Rev. B* 79 (2009) 134415.
- [26] R.L. Antón, J.A. González, J.P. Andrés, J. Canales-Vázquez, J.A. De Toro, J.M. Riveiro, *Nanotechnology* 25 (2014) 105702.
- [27] D. Fiorani, L. Del Bianco, A.M. Testa, K.N. Trohidou, *Phys. Rev. B* 73 (2006) 092403.
- [28] S.E. Inderhees, J.A. Borchers, K.S. Green, M.S. Kim, K. Sun, G.L. Strycker, M.C. Aronson, *Phys. Rev. Lett.* 101 (2008) 117202.
- [29] Y.J. Tang, D.J. Smith, B.L. Zink, F. Hellman, A.E. Berkowitz, *Phys. Rev. B* 67 (2003) 054408.
- [30] M. Gruyters, D. Riegel, *Phys. Rev. B* 63 (2000) 052401.
- [31] J. Denardin, M. Knobel, L. Dorneles, L. Schelp, *J. Magn. Magn. Mater.* 294 (2005) 206–212.
- [32] C.T. Campbell, *Surf. Sci. Rep.* 27 (1997) 1–111.
- [33] X. Chen, S. Bedanta, O. Petravic, W. Kleemann, S. Sahoo, S. Cardoso, P.P. Freitas, *Phys. Rev. B* 72 (2005) 214436.
- [34] F. Luis, J.M. Torres, L.M. García, J. Bartolomé, J. Stankiewicz, F. Petroff, F. Fetta, J.-L. Maurice, A. Vaurès, *Phys. Rev. B* 65 (2002) 094409.
- [35] J.-L. Maurice, J. Briatico, J. Carrey, F. Petroff, L.F. Schelp, A. Vaurès, *Philos. Mag. A* 79 (1999) 2921–2934.
- [36] J.A. De Toro, J.P. Andrés, J.A. González, P. Muñoz, T. Muñoz, P.S. Normile, J.M. Riveiro, *Phys. Rev. B* 73 (2006) 094449.
- [37] P. Xiong, G. Xiao, J.Q. Wang, J.Q. Xiao, J.S. Jiang, C.L. Chien, *Phys. Rev. Lett.* 69 (1992) 3220–3223.
- [38] A.B. Pakhomov, X. Yan, B. Zhao, *Appl. Phys. Lett.* 67 (1995) 3497.
- [39] S. Laureti, S.Y. Suck, H. Haas, E. Prestat, O. Bourgeois, D. Givord, *Phys. Rev. Lett.* 108 (2012) 077205.
- [40] M.S. Lund, W.A.A. Macedo, K. Liu, J. Nogués, I.K. Schuller, C. Leighton, *Phys. Rev. B* 66 (2002) 054422.
- [41] A. Harres, M. Mikhov, V. Skumryev, A. de Andrade, J. Schmidt, J. Geshev, *J. Magn. Magn. Mater.* 402 (2016) 76–82.
- [42] K. Simeonidis, C. Martínez-Boubeta, O. Iglesias, A. Cabot, M. Angelakeris, S. Mourdikoudis, I. Tsiaoussis, A. Delimitis, C. Dendrinou-Samara, O. Kalogirou, *Phys. Rev. B* 84 (2011) 144430.
- [43] J.C. Denardin, A.L. Brandl, M. Knobel, P. Panissod, A.B. Pakhomov, H. Liu, X.X. Zhang, *Phys. Rev. B* 65 (2002) 064422.